Models for Verdoheme Hydrolysis. Paramagnetic Products from the Ring Opening of Verdohemes, 5-Oxaporphyrin Complexes of Iron(II), with Methoxide Ion

Richard Koerner,[†] Lechosoław Latos-Grażyński,[‡] and Alan L. Balch*,[†]

Contribution from the Department of Chemistry, University of California, Davis, California 95616, and the Department of Chemistry, University of Wrocław, Wrocław, Poland

Received February 18, 1998

Abstract: Studies of the reaction of 5-oxaporphyrin iron complexes (verdohemes) with methoxide ion have been undertaken to provide models for the initial step in hydrolysis of verdohemes. Treatment of both low-spin $[(py)_2Fe^{II}(OEOP)]Cl$ and high-spin $\{ClFe^{II}(OEOP)\}$ (OEOP is the monoanion of octaethyl-5-oxaporphyrin) with methoxide ion in either pyridine or methanol solution is shown to cause ring opening and addition of methoxide to one end of the tetrapyrrole. Black $\{Fe^{II}(OEBOMe)\}_2$ has been isolated in crystalline form from the reaction of $\{ClFe^{II}(OEOP)\}$ with methoxide in methanol and studied by single-crystal X-ray diffraction. The molecule has a centrosymmetric dimeric structure composed of two helical Fe(OEBOMe) units with FeN_4 coordination which are connected by a pair of Fe−O bonds. Each iron ion has approximately trigonal bipyramidal geometry. Evidence is presented which suggests that $\{Fe^{II}(OEBOMe)\}_2$ dissolves in dichloromethane in the presence of methanol or pyridine to form high-spin $\{(MeOH)_nFe^{II}(OEBOMe)\}$ or $\{(py)_n$-$Fe^{II}(OEBOMe)\}$ ($n = 1$ or 2) through rupture of the Fe−O bonds in the dimer. The electronic absorption spectra of these open chain complexes show characteristic low-energy features at ca. 720 and 810 nm. The ^1H NMR spectrum of $\{Fe^{II}(OEBOMe)\}_2$ at 23 °C shows a characteristic upfield methoxy resonance, 16 methylene resonances in the 47 to 5 ppm region, and meso resonances in the 51 to 29 ppm region. The temperature dependence of these spectra shows marked deviations from the Curie law, which are consistent with a dimeric structure.

Introduction

Verdohemes, **1**, are the green iron complexes of the 5-oxaporphyrin macrocycle.[1−3] They are produced chemically by the process of coupled oxidation in which an iron porphyrin is subjected to aerial oxidation in solution in the presence of an excess of axial ligands (pyridine or cyanide ion) and a reducing agent (ascorbic acid or hydrazine).[4,5] Alternatively, verdohemes can be prepared by the cyclization and dehydration of biliverdin, **2**, in the presence of iron salts.[6,7] Verdohemes can also be observed as intermediates in the process of heme degradation catalyzed by heme oxygenase.[8−10] This enzyme acts on heme as a substrate and converts it into biliverdin, free iron ion, and carbon monoxide in an oxidative process that involves the activation of three molecules of dioxygen.[11]

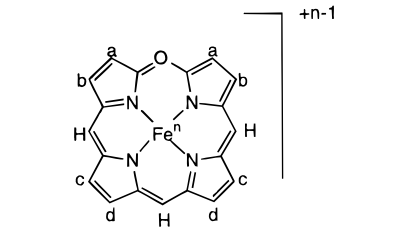

1,
$[Fe^n(OEOP)]^{+n-1}$
a, b, c, d = Et

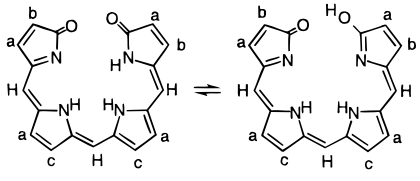

2, biliverdin
a = methyl, b = vinyl, c = propionate
2', H_3OEB,
a = b = c = ethyl

Relatively little is known about the mechanism by which verdoheme is enzymatically converted into biliverdin and

[†] University of California.
[‡] University of Wrocław.

(1) Balch, A. L.; Latos-Grażyński, L.; Noll, B. C.; Olmstead, M. M.; Szterenberg, L.; Safari, N. *J. Am. Chem. Soc.* **1993**, *115*, 1422 and references therein.
(2) Balch, A. L.; Koerner, R.; Olmstead, M. M. *J. Chem. Soc., Chem. Commun.* **1995**, 873−874.
(3) Lagarias, J. C. *Biochim. Biophys. Acta* **1982**, *717*, 12.
(4) Balch, A. L.; Latos-Grażyński, L.; Noll, B. C.; Olmstead, M. M.; Safari, N. *J. Am. Chem. Soc.* **1993**, *115*, 9056 and references therein.
(5) Balch, A. L.; Koerner, R.; Latos-Grażyński, L.; Lewis, J. E.; St. Claire, T. N.; Zovinka, E. P. *Inorg. Chem.* **1997**, *36*, 3892.
(6) Saito, S.; Itano, H. A. *J. Chem. Soc., Perkin Trans. 1* **1986**, 1.
(7) Saito, S.; Sumita, S.; Iwai, K.; Sano, H. *Bull. Chem. Soc. Jpn.* **1988**, *61*, 3539.
(8) Wilks, A.; Ortiz de Montellano, P. R. *J. Biol. Chem.* **1993**, *268*, 22357.
(9) Takahashi, S.; Matera, K. M.; Fujii, H.; Zhou, H.; Ishikawa, K.; Yoshida, T.; Ikeda-Saito, M.; Rousseau, D. L. *Biochemistry* **1997**, *36*, 1402.
(10) Liu, Y.; Moënne-Loccoz, P.; Loehr, T. M.; Ortiz de Montellano, P. R. *J. Biol. Chem.* **1997**, *272*, 6909.
(11) Maines, M. D. *Heme Oxygenase: Clinical Applications and Functions*; CRC Press: Boca Raton, FL, 1992.

S0002-7863(98)00558-7 CCC: $15.00
Published on Web 08/28/1998

Scheme 1[a]

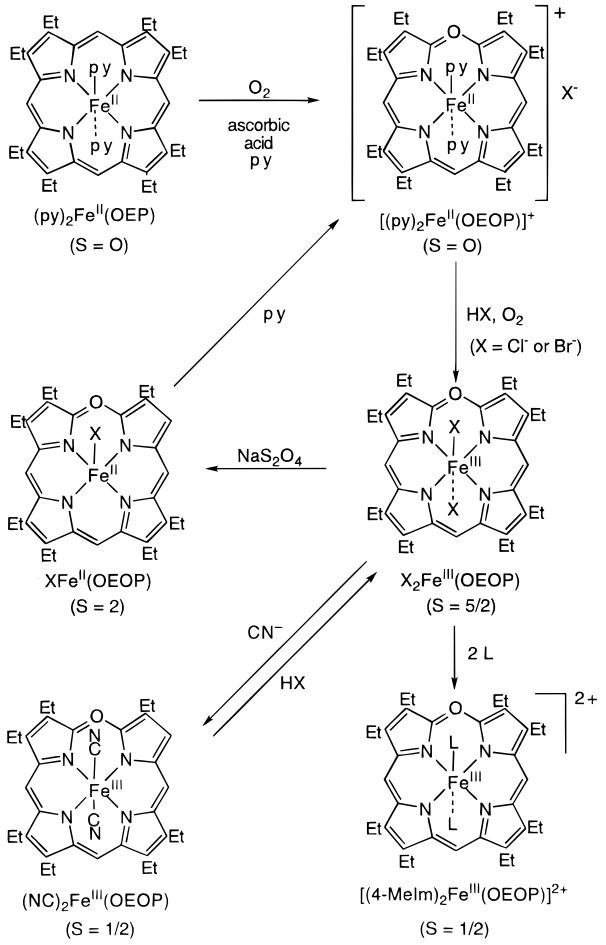

[a] Abbreviations used: (OEP), dianion of octaethylporphyrin; (OEOP), anion of octaethyl-5-oxaporphyrin; (OEB), trianion of octaethylbilindione; (OEBOMe), dianion of octaethylmethoxybiliverdin; py, pyridine.

released from the enzyme. However, it is known that the macrocycle in verdohemes is remarkably stable. Scheme 1 shows a number of chemical transformations that have been observed for well-defined model compounds.[1,2,12] As seen in this scheme, the iron center can undergo a set of reactions that include changes in oxidation state, axial ligation, and spin state. These reactions are analogous to those of metalloporphyrins, and the 5-oxaporphyrin ligand remains intact throughout the transformations shown in this scheme.

Two chemical paths for the conversion of verdohemes into biliverdin have been discussed. These are shown in Scheme 2. One (labeled A) involves hydrolysis of the 5-oxaporphyrin macrocycle; the other (B) utilizes oxidation of the verdoheme.[13−15] The oxidative path results in release of the oxidized iron ion. Although H_3OEB can undergo a 2-electron oxidation,[16] it is not oxidized further in the coupled oxidation process, and heme oxygenase releases biliverdin, not its oxidation product. The hydrolytic pathway is generally considered to begin with addition of hydroxide to the verdoheme. Two possible products of nucleophilic addition to verdoheme that have been generally considered are the closed macrocycle, **3**, and its open chain

Scheme 2

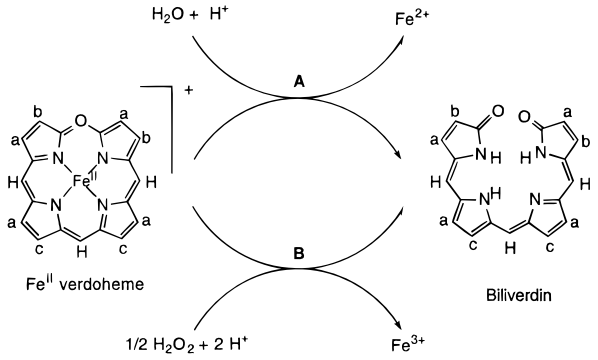

isomer, **4**.[17−21] Since both isomers have C_1 symmetry, symmetry-based NMR spectroscopic methods are not able to clearly identify the exact isomer that is formed. For example, for the

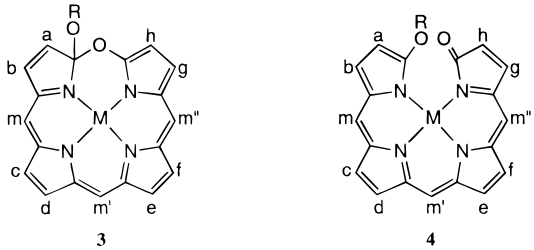

3 **4**

product obtained from $[Fe^{II}(OEOP)]^+$, the ^{1}H NMR spectrum is expected to consist of three meso resonances, eight methyl resonances, sixteen methylene resonances, and one methoxy resonance for either isomer. Moreover, nothing is known about the properties that either structure will confer upon the iron ion at the center. That is, it remains to be seen which oxidation, spin, and ligation states will be stable for either structural form, **3** or **4**.

To characterize the reactivity of verdoheme, especially in regard to reactions that affect the macrocycle itself, we have undertaken the study of the products of methoxide addition to $[Fe^{II}(OEOP)]^+$ in two differently ligated forms. Methoxide, rather that hydroxide, was used so that we could inhibit further deprotonation/protonation reactions that might follow the initial attack. We were particularly concerned with verdohemes in ligation and oxidation states that resemble those found in a protein environment or in the environment used in the coupled oxidation process that has been examined as a model for heme degradation. Consequently, our initial attention was focused on the diamagnetic complex, $[(py)_2Fe^{II}(OEOP)]Cl$, and its reaction with methoxide in pyridine.

Results

Alkoxide Addition to Verdoheme, $[(py)_2Fe^{II}(OEOP)]Cl$. Addition of a solution of potassium hydroxide in methanol or sodium methoxide in methanol to a green, pyridine solution of diamagnetic $[(py)_2Fe^{II}(OEOP)]Cl$ in the absence of dioxygen produces a yellow brown, air-sensitive solution. The ^{1}H NMR spectrum of the resulting solution prepared from pyridine-d_5

(12) Balch, A. L.; Noll, B. C.; Safari, N. *Inorg. Chem.* **1993**, *32*, 2901.
(13) Hirota, T.; Itano, H. A. *Tetrahedron Lett.* **1983**, *24*, 995.
(14) Sano, S.; Sano, T.; Morishima, I.; Shiro, Y.; Maeda, Y. *Proc. Natl. Acad. Sci. U.S.A.* **1986**, *83*, 531.
(15) Saito, S.; Itano, H. A. *Proc. Natl. Acad. Sci. U.S.A.* **1982**, *79*, 1393.
(16) Balch, A. L.; Koerner, R.; Olmstead, M. M.; Safari, N.; St. Claire, T. *J. Chem. Soc., Chem. Commun.* **1995**, 643.
(17) Fuhrhop, J.-H.; Salek, A.; Subramanian, J.; Mengersen, C.; Besecke, S. *Leibigs Ann. Chem.* **1975**, 1131.
(18) Fuhrhop, J.-H.; Krüger, P.; Sheldrick, W. S. *Leibigs Ann. Chem.* **1977**, 339.
(19) Fuhrhop, J.-H.; Krüger, P. *Liebigs Ann. Chem.* **1977**, 360.
(20) Hempenius, M. A.; Koek, J. H.; Lugtenburg, J.; Fokkens, R. *Recl. Trav. Chim. Pays-Bas* **1987**, *106*, 105.
(21) Mizutani, T.; Yagi, S.; Honmaru, A.; Ogoshi, H. *J. Am. Chem. Soc.* **1996**, *118*, 5318.

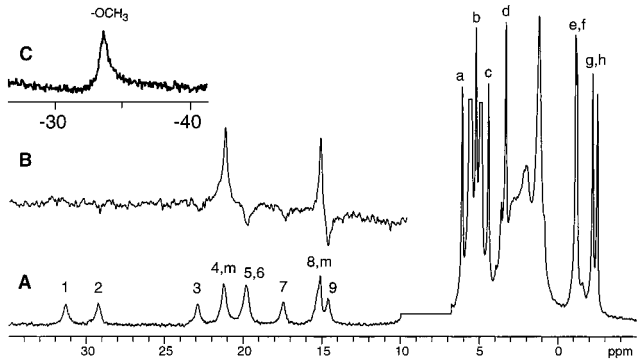

Figure 1. (A) The 300 MHz ^{1}H NMR spectrum (under inversion recovery conditions with τ = 100 ms) of a solution of diamagnetic [(py)$_2$Fe^{II}(OEOP)]Cl in pyridine-d_5 after the addition of a solution of sodium methoxide-d_3 in methanol-d_4. (B) The same spectrum with τ = 10 ms to observe the meso resonances. (C) The upfield region from a sample prepared by the addition of undeuterated sodium methoxide in normal methanol. No resonances are observed in this region in the spectrum when deuterated methanol and methoxide are used. Resonances are assigned with the following labels: m for the meso protons, letters a−h for the methyl protons of the ethyl groups, numbers for the methylene protons, and OCH_3 for the methoxy protons.

and methanol-d_4 is shown in Trace A of Figure 1 with the methoxide present in 1 equiv excess. This spectrum clearly indicates that a new, paramagnetic species is present, but otherwise the spectral information available is limited. For example, the meso resonances, which usually can be easily identified on the basis of their greater line width (due to their proximity to the iron), are not readily apparent. However, under inversion recovery conditions with a shorter τ value, two resonances which are presumed to be meso resonances are detected at 15 and 21.4 ppm as seen in Trace B of Figure 1. Eight resonances in the 7 to −3 ppm region are assigned to the methyl protons on the basis of their intensities, and the eight resonances in the 14 to 32 ppm region are likely to be due to methylene protons. When the sample is prepared with undeuterated methoxide and methanol, a new resonance is observed at −34 ppm as seen in Trace C of Figure 1. This apparently arises from methoxide or methanol that is somehow added to the verdoheme, either through coordination to iron or by addition to the ligand. Numerous attempts to isolate the species responsible for the spectra shown in Figure 1 from pyridine solution by precipitation, crystallization, or chromatographic separation have not been successful. Consequently, identification of the species responsible for the spectral features shown in Figure 1 has had to rely on another approach.

Alkoxide Addition to ClFe^{II}(OEOP) and the Formation of {Fe^{II}(OEBOMe)}$_2$. Addition of sodium methoxide in methanol to a methanol solution of ClFe^{II}(OEOP) in the absence of dioxygen produces a marked color change from deep green to yellow green. Concentration and storage of the solution results in the precipitation of the product, {Fe^{II}(OEBOMe)}$_2$, as black crystals in remarkably pure form. The choice of solvent for this procedure is particularly crucial. Although ClFe^{II}(OEOP) has good solubility in dichloromethane and chloroform and reacts with sodium methoxide in methanol in these solvents, the resulting solutions have limited stability possibly due to side reactions initiated by reactions of the added base with the chlorocarbons.

Crystalline {Fe^{II}(OEBOMe)}$_2$ is air stable for days and has good solubility in chloroform and dichloromethane. These solutions are sensitive to air and have been handled under a dinitrogen atmosphere. Although {(CH$_3$OH)$_n$Fe^{II}(OEBOMe)}

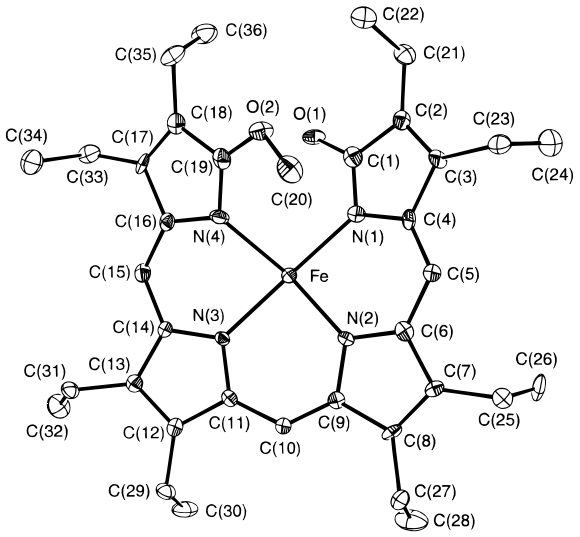

Figure 2. A perspective drawing of the asymmetric unit in {Fe^{II}(OEBOMe)}$_2$, which shows the numbering scheme, with 50% thermal ellipsoids.

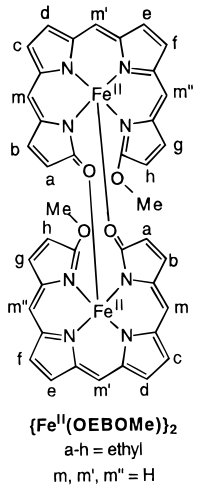

is soluble in methanol when initially formed, once {Fe^{II}(OEBOMe)}$_2$ is obtained in crystalline form, it does not redissolve in methanol. It is also very poorly soluble in pyridine.

X-ray Crystallographic Analysis of the Structure of {Fe^{II}(OEBOMe)}$_2$. The asymmetric unit, which is shown in Figure 2, constitutes one-half of the dimeric molecule. Two helical Fe^{II}(OEBOMe) units are positioned about a center of symmetry to form the complete dimeric molecule. Two perspective views of the entire molecule are shown in Figure 3. Table 1 presents selected bond distances and angles for the dimer.

Each iron atom in the dimer is five-coordinate with bonds to four nitrogen atoms in one tetrapyrrole unit and a bond to an oxygen atom in the adjacent tetrapyrrole. The coordination geometry about iron approximates a trigonal bipyramid. The axial portion is comprised of the N(1)−Fe−N(3) segment, which has a nearly linear geometry (bond angle, 170.2(2)°). Within the equatorial plane, the N(2)−Fe−N(4) angle (134.2(2)°) is wider and the O(1)−Fe−N(4) angles (113.612 and 111.5(2)°, respectively) are narrower than the expected 120°. The sum of these three bond angles is 359.3°, so the FeO(1)N(2)N(4) unit is nearly planar. The bond angles at iron between the axial and equatorial donors fall into a reasonably narrow range, 82.3−96.1°, that is near the ideal of 90°.

The Fe−N bond distances in {Fe^{II}(OEBOMe)}$_2$ span the range 2.092(5)−2.205(5) Å. For comparison, the Fe−N

distances in typical Fe^{II} porphyrins fall in the range 2.07−2.10 Å.[22,23] Longer Fe−N bonds are found in complexes of modified porphyrins such as N-alkylated porphyrins where the Fe−N distances fall in the range 2.08−2.51°.[24,25] The Fe−O distance, 2.020(14) Å, is, as usual, longer than the corresponding Fe−N distances.

Comparison between the structures of $\{Fe^{II}(OEBOMe)\}_2$ and $\{Fe^{III}(OEB)\}_2$,[4] the iron(III) complex of octaethylbilindione (**2′**), is informative. Figure 4 shows a superposition of the two

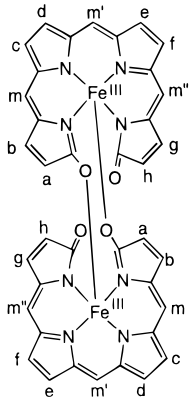

{Fe^{III}(OEB)}$_2$
a-h = ethyl
m, m', m" = H

structures. Both are dimers in which the helical asymmetric units are arranged about a crystallographic center of symmetry to produce the entire molecule. The Fe−N and Fe−O distances in the iron(II) complex, $\{Fe^{II}(OEBOMe)\}_2$ (Fe−N range, 2.092(5)−2.205(5) Å; Fe−O, 2.020(14) Å), are longer than those in the iron(III) complex, $\{Fe^{III}(OEB)\}_2$ (Fe−N range, 2.0323(15)−2.160(13) Å; Fe−O, 1.911(16) Å). In $\{Fe^{III}(OEB)\}_2$ the iron site is only partially occupied (refined fractional occupancy 0.56) and the crystal is apparently comprised of a mixture of $\{Fe^{III}(OEB)\}_2$ and $\{Fe^{III}(HOEB)(H_2OEB)\}$ in which an O-bound $[H_2OEB]^-$ group acts as the axial ligand to the iron atom which resides at the center of a helical $[HOEB]^{2-}$ ligand that is coordinated through its four pyrrole nitrogen atoms.[4] This partial occupancy of the iron site in crystalline $\{Fe^{III}(OEB)\}_2$ is entirely consistent with its chemical behavior. Dimeric $\{Fe^{III}(OEB)\}_2$ is readily demetalated, and efforts to prepare it by reaction of iron compounds with the free ligand, H_3OEB, have not met with success. The structure of $\{Fe^{II}(OEBOMe)\}_2$ does not suffer from this problem: the site of the iron atom is fully occupied.

Inspection of the structures of the Fe-pyrrole units within $\{Fe^{II}(OEBOMe)\}_2$ reveals an unusual tilting. Ideally the iron atom should reside in the plane of the pyrrole group to which it is coordinated. However, in $\{Fe^{II}(OEBOMe)\}_2$ there is considerable distortion within these units. Relevant data, in the form of displacements of the iron atom from the plane of the coordinated pyrrole rings and angles between the Fe−N bond and the plane of the coordinated pyrrole, are given in Table 2. Each Fe-pyrrole unit shows some distortion from the expected geometry. This distortion is greatest for the pyrrole ring that contains N(4), i.e. the terminal pyrrole ring with the appended methoxy group. For this pyrrole ring, the iron atom is 1.33 Å

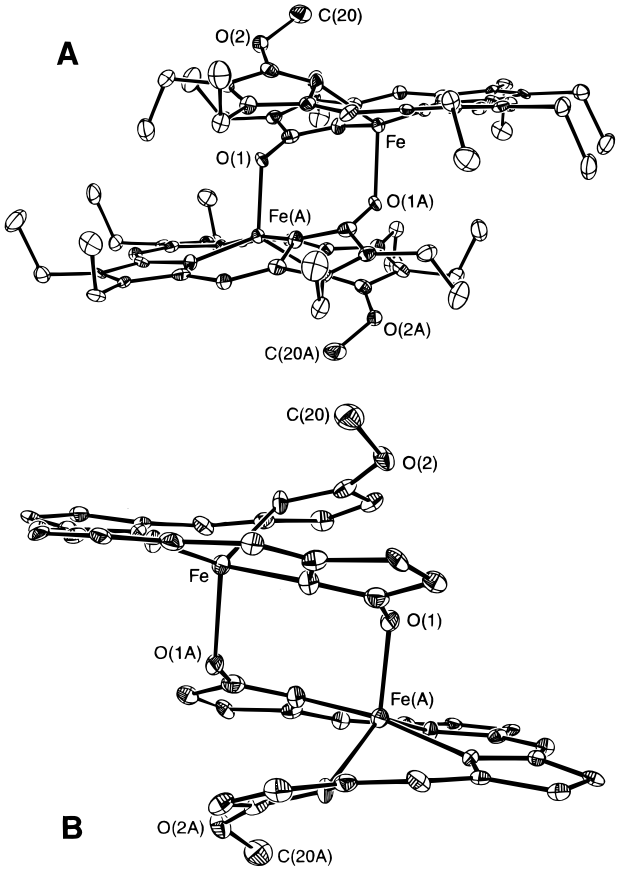

Figure 3. Two views of $\{Fe^{II}(OEBOMe)\}_2$. Part A shows the orientation of the ethyl groups. In part B, the ethyl groups are removed to emphasize the helical nature of the inner core.

out of the plane and the Fe−N bond is bent 36.2° out of the pyrrole plane. Note also that the Fe−N(4) bond is the longest of the four Fe−N bonds in the complex. To assess the significance of these distortions, Table 2 presents complementary information on several related complexes.[1,26] These data show that a wide range of displacements of the metal ion from the pyrrole plane occur in related complexes, but that the displacements for $\{Fe^{II}(OEBOMe)\}_2$ are unusually large. The structure of $\{Fe^{III}(OEB)\}_2$ shows similar displacements. Thus, the cause of these distortions cannot be traced to the electronic structures of these Fe(II) and Fe(III) complexes. The tilting of analogous groups, particularly thiophene rings, is common in heteroporphyrin structures, but in these complexes the pyrrole rings do not display abnormal tilting.[27,28]

Spectroscopic and Electrochemical Studies of the Behavior of $\{Fe^{II}(OEBOMe)\}_2$ in Solution. Trace B of Figure 5 shows the UV/vis absorption spectrum of $\{Fe^{II}(OEBOMe)\}_2$ in dichloromethane solution, while Inset A shows the UV/vis spectrum of verdoheme, $[(py)_2Fe^{II}(OEOP)]Cl$, for comparison. The characteristic verdoheme peak at 662 nm for $ClFe^{II}(OEOP)$ is absent,[1] but new, broad bands are seen at longer wavelength. The absorption spectra of solutions of $\{Fe^{II}(OEBOMe)\}_2$ are sensitive to the presence of potential axial ligands. Trace C of Figure 2 shows the effect of the addition of methanol to a dichloromethane solution of $\{Fe^{II}(OEBOMe)\}_2$. The addition

(22) Scheidt, R. W.; Reed, C. A. *Chem. Rev.* **1981**, *81*, 543.
(23) Scheidt, W. R.; Lee, Y. J. *Struct. Bonding* **1987**, *64*, 1.
(24) Anderson, O. A.; Kopelove, A. B.; Lavallee, D. K. *Inorg. Chem.* **1980**, *19*, 2101.
(25) Balch, A. L.; Chan, Y. W.; Olmstead, M. M.; Renner, M. W. *J. Org. Chem.* **1986**, *51*, 4651.
(26) Balch, A. L.; Manzzanti, M.; Noll, B. C.; Olmstead, M. M. *J. Am. Chem. Soc.* **1994**, *116*, 9114.
(27) Latos-Grażyński, L.; Lisowski, J.; Olmstead, M. M.; Balch, A. L. *J. Am. Chem. Soc.* **1987**, *109*, 4428.
(28) Latos-Grażyński, L.; Lisowski, J.; Olmstead, M. M.; Balch, A. L. *Inorg. Chem.* **1989**, *28*, 1183.

Table 1. Selected Bond Lengths (Å) and Angles (deg) for $\{Fe^{II}(OEBOCH_3)\}_2$

Bond Lengths			
Fe−O(1)	2.020(4)	Fe−N(2)	2.092(5)
Fe−N(1)	2.101(5)	Fe−N(3)	2.111(5)
Fe−N(4)	2.205(5)	N(1)−C(1)	1.353(7)
N(1)−C(4)	1.391(7)	N(2)−C(6)	1.349(7)
N(2)−C(9)	1.391(7)	N(3)−C(14)	1.357(7)
N(3)−C(11)	1.372(7)	N(4)−C(19)	1.321(7)
N(4)−C(16)	1.442(7)	O(1)−C(1)	1.286(7)
O(2)−C(19)	1.339(7)	O(2)−C(20)	1.431(7)
C(1)−C(2)	1.483(8)	C(2)−C(3)	1.347(8)
C(3)−C(4)	1.480(8)	C(4)−C(5)	1.357(8)
C(5)−C(6)	1.436(8)	C(6)−C(7)	1.432(8)
C(7)−C(8)	1.369(8)	C(8)−C(9)	1.445(8)
C(9)−C(10)	1.381(7)	C(10)−C(11)	1.402(8)
C(11)−C(12)	1.439(7)	C(12)−C(13)	1.379(8)
C(13)−C(14)	1.432(7)	C(14)−C(15)	1.421(8)
C(15)−C(16)	1.353(8)	C(16)−C(17)	1.464(8)
C(17)−C(18)	1.354(8)	C(18)−C(19)	1.457(8)
Angles			
N(1)−Fe−N(2)	87.9(2)	N(2)−Fe−N(3)	87.3(2)
N(3)−Fe−N(4)	82.3(2)	N(1)−Fe−N(4)	95.0(2)
N(1)−Fe−N(3)	170.2(2)	N(2)−Fe−N(4)	134.2(2)
O(1)−Fe−N(1)	96.1(2)	O(1)−Fe−N(2)	113.6(2)
O(1)−Fe−N(3)	93.6(2)	O(1)−Fe−N(4)	111.5(2)
C(1)−N(1)−C(4)	105.9(5)	C(1)−N(1)−Fe	126.4(4)
C(4)−N(1)−Fe	125.7(4)	C(6)−N(2)−C(9)	106.2(5)
C(6)−N(2)−Fe	127.4(4)	C(9)−N(2)−Fe	125.3(4)
C(14)−N(3)−C(11)	105.9(5)	C(14)−N(3)−Fe	126.7(4)
C(11)−N(3)−Fe	126.4(4)	C(19)−N(4)−C(16)	103.6(5)
C(19)−N(4)−Fe	129.3(4)	C(16)−N(4)−Fe	112.6(3)
C(1)−O(1)−Fe	126.8(4)	C(19)−O(2)−C(20)	117.5(4)
O(1)−C(1)−N(1)	124.3(5)	O(1)−C(1)−C(2)	124.4(5)
N(1)−C(1)−C(2)	111.4(5)	C(3)−C(2)−C(1)	105.8(5)
C(2)−C(3)−C(4)	107.3(5)	C(5)−C(4)−N(1)	124.1(5)
C(5)−C(4)−C(3)	126.3(5)	N(1)−C(4)−C(3)	109.5(5)
C(4)−C(5)−C(6)	127.7(6)	N(2)−C(6)−C(7)	111.2(5)
N(2)−C(6)−C(5)	123.6(5)	C(7)−C(6)−C(5)	125.2(5)
C(8)−C(7)−C(6)	106.7(5)	C(7)−C(8)−C(9)	106.5(5)
C(10)−C(9)−N(2)	124.5(5)	C(10)−C(9)−C(8)	126.2(5)
N(2)−C(9)−C(8)	109.3(5)	C(9)−C(10)−C(11)	128.9(5)
N(3)−C(11)−C(10)	122.8(5)	N(3)−C(11)−C(12)	110.5(5)
C(10)−C(11)−C(12)	126.5(5)	C(13)−C(12)−C(11)	106.2(5)
C(12)−C(13)−C(14)	106.2(5)	N(3)−C(14)−C(15)	121.6(5)
N(3)−C(14)−C(13)	111.3(5)	C(15)−C(14)−C(13)	127.1(5)
C(16)−C(15)−C(14)	127.0(6)	C(15)−C(16)−N(4)	122.9(5)
C(15)−C(16)−C(17)	126.9(6)	N(4)−C(16)−C(17)	109.4(5)
C(18)−C(17)−C(16)	106.7(5)	C(17)−C(18)−C(19)	105.8(5)
N(4)−C(19)−O(2)	125.4(5)	N(4)−C(19)−C(18)	114.2(5)
O(2)−C(19)−C(18)	120.3(5)		

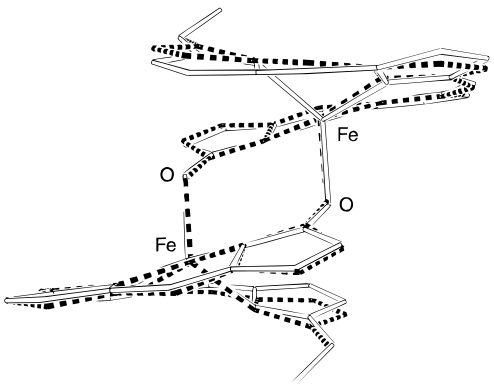

Figure 4. A comparison of the inner cores of $\{Fe^{II}(OEBOMe)\}_2$ (represented by open lines) and $\{Fe^{III}(OEB)\}_2$ (represented by dashed lines).

of pyridine to a solution of $\{Fe^{II}(OEBOMe)\}_2$ in dichloromethane produces a similar change in the UV/vis spectrum as shown in Trace D of Figure 5. These changes are indicative

Table 2. Arrangements of Metal-Pyrrole Coordination

compd	displacement of M from pyrrole mean plane (Å)		M−N to pyrrole plane angle (deg)
$\{Fe^{II}(OEBOMe)\}_2$	0.56	C═O[a]	15.0
(this work)	0.35		9.5
	0.31		8.7
	1.33	COMe	36.2
$\{Fe^{II}(OEB)\}_2$	0.78	C═O	21.1
(ref 4)	0.16		4.8
	0.72		19.5
	1.22	C−O−Fe	32.6
$\{Mn^{III}(OEB)\}_2$	0.16	C═O	4.4
(ref 26)	0.27		7.7
	0.31		9.0
	0.40	C−O−Mn	11.0
$ClFe^{II}(OEOP)$	0.40		10.8
(ref 1)	0.45		12.1
	0.60		16.3
	0.30		8.5

[a] Designates the terminal pyrrole ring involved.

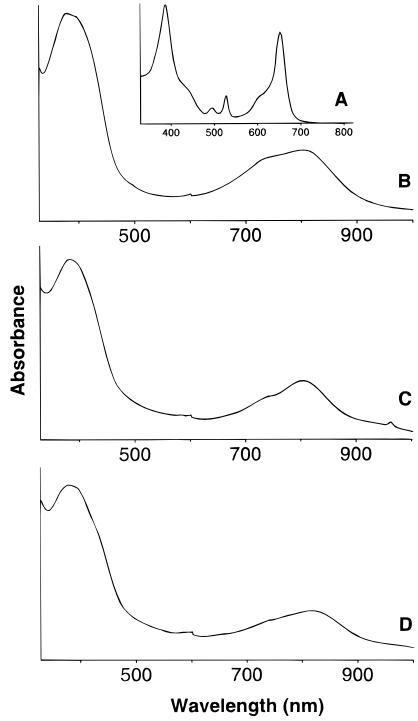

Figure 5. Electronic absorption spectra of (B) $\{Fe^{II}(OEBOMe)\}_2$ in dichloromethane solution [λ_{max}, nm (ϵ, M^{-1} cm^{-1} per dimer): 380 (5.9×10^4), 388 (5.8×10^4), 728 (1.7×10^4), 804 (2.0×10^4)]; (C) $\{Fe^{II}(OEBOMe)\}_2$ in dichloromethane solution with 1 vol % of methanol added ($\{(MeOH)_nFe^{II}(OEBOMe)\}$ is present) [λ_{max}, nm (ϵ, M^{-1} cm^{-1} per iron): 382 (2.8×10^4), 724 (7.3×10^3), 804 (1.0×10^4)]; and (D) $\{Fe^{II}(OEBOMe)\}_2$ in dichloromethane solution with 1 vol % of pyridine added ($\{(py)_nFe^{II}(OEBOMe)\}$ is present) [λ_{max}, nm (ϵ, M^{-1} cm^{-1} per iron): 380 (2.8×10^4), 744 (7.2×10^3), 818 (8.5×10^3)]. Insert A shows the UV/vis spectrum of verdoheme, $[(py)_2Fe^{II}(OEOP)]Cl$, for comparison.

of cleavage of the dimeric $\{Fe^{II}(OEBOMe)\}_2$, and coordination of methanol or pyridine in place of the axial Fe−O bonds in $\{Fe^{II}(OEBOMe)\}_2$.

The ^1H NMR spectrum of $\{Fe^{II}(OEBOMe)\}_2$ in dichloromethane solution is shown in Trace A of Figure 6. Assignment of the spectrum on the basis of line widths and relative intensities is relatively straightforward. In the 11 to 4 ppm region the eight, equally intense resonances, which are the narrowest resonances in the paramagnetic part of the spectrum, are assigned to the methyl protons. Sixteen resonances (labeled

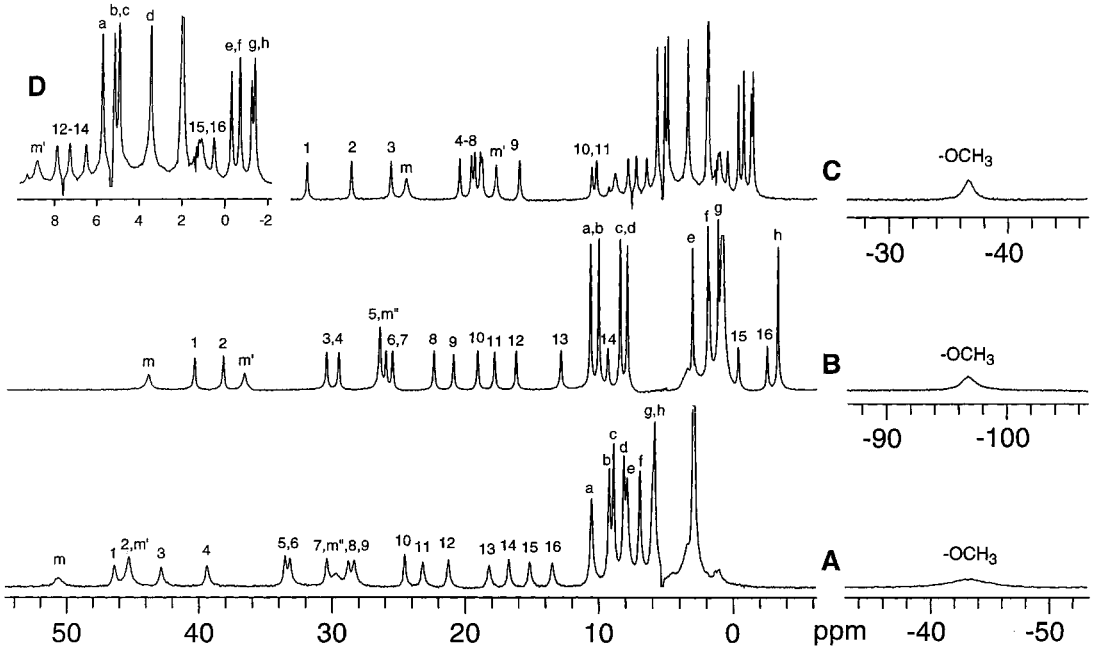

Figure 6. The 300 MHz ^{1}H NMR spectra of (A) {Fe^{II}(OEBOMe)}$_2$ in dichloromethane-d_2 solution, (B) {Fe^{II}(OEBOMe)}$_2$ in dichloromethane-d_2 with the addition of 1% methanol-d_4; and (C) {Fe^{II}(OEBOMe)}$_2$ in dichloromethane-d_2 with the addition of 1% pyridine-d_5. Spectrum D shows the crowded 10 to −2 ppm region. All spectra were collected under inversion recovery conditions with $\tau = 100$ ms. Solvent resonances are inverted and truncated. Individual resonances are labeled with the scheme outlined in the caption to Figure 1.

1 to 16) are assigned to the methylene protons. The two broadest resonances, at 50.5 and 29.8 ppm (labeled m and m′), are assigned to the meso protons. The third meso resonance is coincident with one of the methylene resonances at 45.5 ppm. The assignment of the meso protons has been confirmed by observation of the ^{1}H and ^{2}H NMR spectra of a sample of meso-deuterated {Fe^{II}(OEBOMe)}$_2$ that was prepared from meso-deuterated ClFe^{II}(OEOP). Although we have been able to differentiate and assign the meso, methylene, and methyl resonances, assignments of individual resonances to specific protons within the complex are not possible with the data presented here. A unique resonance at −43.5 ppm is assigned to the methoxy protons. This peak is absent from spectra taken of the complex when it is prepared from methoxide-d_3. The temperature dependencies of the chemical shifts for the meso protons and the methoxy proton of {Fe^{II}(OEBOMe)}$_2$ are shown in Figure 7. The plots show significant deviation from the Curie law. The other resonances also exhibit variations with temperature that do not follow the Curie law, but to keep Figure 7 reasonably clear, the behaviors of the other resonances are not shown.

The ^{1}H NMR spectrum of {Fe^{II}(OEBOMe)}$_2$, like the UV/vis spectrum described above, is sensitive to the presence of methanol or pyridine. Trace B in Figure 6 shows the effect on the spectrum of the addition of methanol-d_4 to the sample of {Fe^{II}(OEBOMe)}$_2$. Methanol addition produces a narrowing of the line widths of all resonances and changes in their chemical shifts. Nevertheless, the overall pattern of the resonances is similar with the broad meso resonances in downfield positions and the methoxy group resonance in an upfield location, but two of the methylene resonances are shifted upfield of 0 ppm. Note that the methoxy resonance has undergone a pronounced upfield shift when methanol is present. However, exchange between the methoxy group protons in the complex and deuterium in the solvent (methanol-d_4) is slow. No deuterium incorporation into the complex is observed for a sample in methanol-d_4/dichloromethane over 2 days of observation.

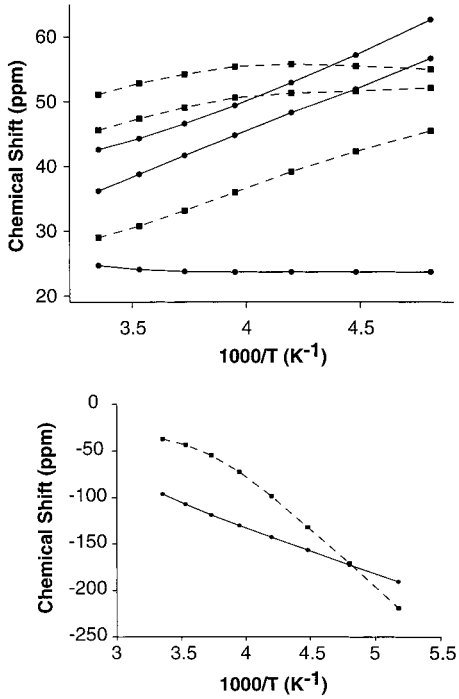

Figure 7. A plot of the chemical shifts of the meso and methoxy resonances for the ^{1}H NMR spectrum of {Fe^{II}(OEBOMe)}$_2$ in dichloromethane solution (squares) and in dichloromethane with 1% methanol added (circles). The lines are drawn solely to clarify the interrelationships between the experimentally determined points.

The temperature dependencies of the chemical shifts for the meso protons and the methoxy proton of {Fe^{II}(OEBOMe)}$_2$ in dichloromethane/methanol solution are shown in Figure 7. In comparison to the behavior of the corresponding resonances of the dichloromethane solution of {Fe^{II}(OEBOMe)}$_2$, the resonances from the dichloromethane/methanol solution show nearly linear behavior.

Trace C in Figure 6 shows the effect of the addition of

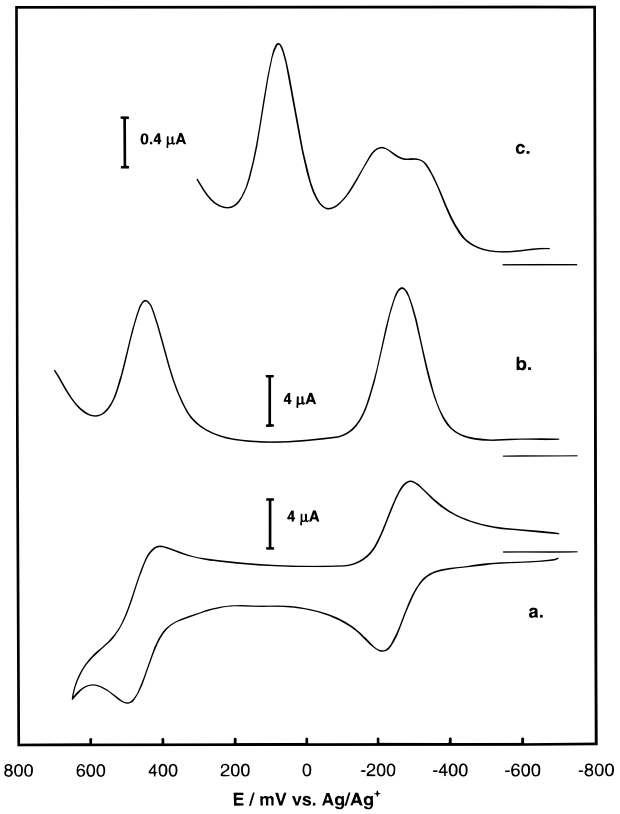

Figure 8. (a) Cyclic voltammogram for a solution of $\{Fe^{II}(OEBOMe)\}_2$ in 4/1 v/v dichloromethane/methanol with tetra(*n*-butyl)ammonium perchlorate as supporting electrolyte at a gold electrode. (b) The square wave voltammogram for the same solution. (c) The square wave voltammogram for a solution of $\{Fe^{II}(OEBOMe)\}_2$ in dichloromethane. All potentials are referenced to the Ag/Ag^+ couple.

pyridine to a sample of $\{Fe^{II}(OEBOMe)\}_2$. The resonances in the spectrum taken in the presence of pyridine are narrowed when compared to those in Trace A of the same figure. Additionally, the chemical shifts of the individual resonances are altered by the addition of pyridine. Although $\{Fe^{II}(OEBOMe)\}_2$ is not very soluble in pyridine, it does slowly dissolve in a pyridine/dichloromethane (9/1 v/v) mixture. The ^1H NMR spectrum of that solution is nearly identical to the spectrum shown in Trace A of Figure 1, except that the upfield methoxy resonance is observed. Thus the species responsible for the spectrum shown in Figure 1 is that of $\{(py)_nFe^{II}(OEBOMe)\}$.

The magnetic moment of $\{Fe^{II}(OEBOMe)\}_2$ in dichloromethane solution is 4.1(3) μ_B per iron at 19.7 °C. This value is lower than the spin only value of 4.9 μ_β predicted for a high-spin d^6 complex of Fe(II). The magnetic moment of $\{Fe^{II}(OEBOMe)\}_2$ in dichloromethane/methanol is 4.6(3) μ_B per iron at 19.7 °C. Note that this value is somewhat larger than that recorded from a solution of the complex in dichloromethane alone.

Electrochemical data for solutions of $\{Fe^{II}(OEBOMe)\}_2$ are presented in Figure 8. Trace a shows the cyclic voltammogram for a solution of $\{Fe^{II}(OEBOMe)\}_2$ in dichloromethane/methanol 4/1 (v/v) with 0.1 M tetra(*n*-butyl)ammonium perchlorate as the supporting electrolyte. Two, reversible oxidation waves are observed. Trace b shows the corresponding square wave voltammograms from the same sample. Trace c of Figure 8 shows the square wave voltammogram of $\{Fe^{II}(OEBOMe)\}_2$ in dichloromethane with 0.1 M tetra(*n*-butyl)ammonium perchlorate as the supporting electrolyte. In the presence of methanol (Traces a and b), two redox processes are observed. In the absence of methanol (Trace c), three redox processes are seen and the first two oxidations have equal currents which are one-half as large as that of the final oxidation. The first two oxidation processes in Trace c are likely to be due to the stepwise Fe(II) to Fe(III) oxidation of each of the two iron centers within dimeric $\{Fe^{II}(OEBOMe)\}_2$. While the first oxidation process seen in Traces a and b of Figure 8 is assigned to the Fe(II) to Fe(III) oxidation of the monomeric form of the complex, further work is necessary to establish whether the second oxidation process seen in Traces a and b and the third oxidation process seen in Trace c are metal or ligand based.

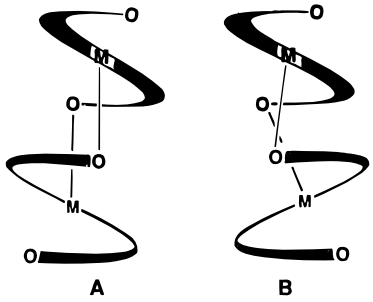

Figure 9. Schematic drawings of isomeric structures for dimers formed by two helical subunits: (**A**) centrosymmetric dimer with the two subunits of opposite chirality and (**B**) C_2-symmetric dimer with two subunits of like chirality.

Discussion

The present study shows that the 5-oxaporphyrin macrocycles in both low-spin and high-spin iron(II) verdohemes undergo addition of methoxide to the verdoheme ligand to produce new paramagnetic complexes that contain a ring-opened tetrapyrrole, i.e. structure **4** above. To date no compound with the isomeric structure **3**, which at one time was proposed as a structural possibility for verdoheme itself,[3,29] has been crystallographically characterized. In the solid state, the product of methoxide addition in methanol solution is the dimer, $\{Fe^{II}(OEBOMe)\}_2$. Within the dimer, each tetrapyrrole unit coordinates to an iron(II) via the four nitrogen atoms to give helical units which are joined by two equivalent Fe−O bonds as shown in Figure 3.

Other types of tetrapyrroles form dimeric structures that are closely related to that of $\{Fe^{II}(OEBOMe)\}_2$. One of these is the biliverdin analogue, octaethylbilindione.[4,26] This ligand can coordinate to a single metal ion to give monomeric, helical complexes with the tetrapyrrole providing four ligating nitrogen atoms or it can act as a bridging ligand in which it coordinates to one metal ion through the usual four nitrogen atoms and to a second through one of the two oxygen atoms as in $\{Fe^{III}(OEB)\}_2$. Complexes in which octaethylbilindione acts as a bridging ligand are currently restricted to cases where M(III) is involved, i.e. Fe^{III} and Mn^{III}.[4,26]

The formation of dimeric molecules by association of two helical subunits through M−O bonds as seen in $\{Fe^{II}(OEBOMe)\}_2$ can produce two different isomeric structures. These are shown schematically in Figure 9. In one (labeled A) the two helices have opposite chirality and dimerize about a center of symmetry. That is the situation seen here for $\{Fe^{II}(OEBOMe)\}_2$ and observed earlier for $\{Fe^{III}(OEB)\}_2$. In the other structure (B), the two helical units that dimerize have like chirality and the resulting molecule is chiral. $\{Mn^{III}(OEB)\}_2$ dimerizes in this fashion.[26] However, the local coordination

(29) Modi, S.; Behere, D. V.; Shedbalkar, V. P. *J. Chem. Res.* **1988**, 244.

environments in the manganese and iron complexes are similar with approximate trigonal bipyramidal geometry and MN_4O coordination.

Another tetrapyrrole that can act as a bridging ligand is the 5-hydroxyporphyrin or oxophlorin. This ligand also has the capability of coordination to a single metal ion through the four nitrogen atoms or coordination to two metal ions through formation of a bridge to a second metal with the use of the peripheral oxygen atom as a donor.[30−32] In the latter case, binuclear species such as $\{M^{III}(OEPO)\}_2$ result.[33−36] Again, the formation of such dimeric entities is so far restricted to complexes of M(III), *i.e.* Fe^{III}, Mn^{III}, Ga^{III}, and In^{III}. In both $\{Fe^{III}(OEB)\}_2$ and $\{Fe^{III}(OEPO)\}_2$, the oxygen donors bear a significant partial negative charge and can act as alkoxide

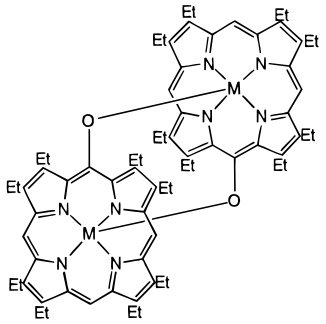

donors. In contrast, in $\{Fe^{II}(OEBOMe)\}_2$ the O−C bond is shorter (1.286(7) Å), and the oxygen atom is in an environment more like that of a keto group. It is well recognized that keto groups generally function poorly as ligands to metal ions such as iron, thus it is unexpected that Fe(II) forms such a binuclear entity as a $\{Fe^{II}(OEBOMe)\}_2$.

Finally, there are two other modified porphyrins that bear hydroxy substituents that form polymeric structures with the resulting alkoxy groups acting as bridges. Insertion of iron into 5-(2-hydroxyphenyl)-10,15,20-tri(tolyl)porphyrin (H_2TTOP) results in the formation of the high-spin, doubly alkoxy-bridged dimer, $\{Fe^{III}(TTOP)\}_2$.[37,38] The 2-hydroxy-5,10,15,20-tetra(phenyl)porphyrin bears a hydroxy group on one of the β-pyrrole positions and forms a series of alkoxy-bridged trimers with Fe(III), Mn(III), and Ga(III).[39−42]

The spectral and electrochemical changes seen when methanol or pyridine are present in solutions made from $\{Fe^{II}(OEBOMe)\}_2$ suggests that these solvents coordinate to the iron, and it is likely that the dimer dissociates via eq 1 to give a

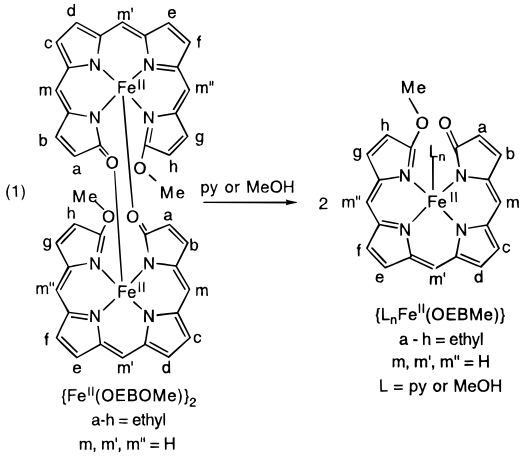

monomeric species (either $\{(MeOH)_nFe^{II}(OEBOMe)\}$ or $\{(py)_nFe^{II}(OEBOMe)\}$ where n is 1 or 2). Similar behavior (e.g. cleavage in the presence of pyridine) is seen for both $\{M^{III}(OEB)\}_2$ and $\{M^{III}(OEPO)\}_2$ as shown in eqs 2[4,24] and 3.[30,31] The evidence that the solvated monomers, $\{(MeOH)_nFe^{II}(OEBOMe)\}$ or $\{(py)_nFe^{II}(OEBOMe)\}$, are formed in the presence

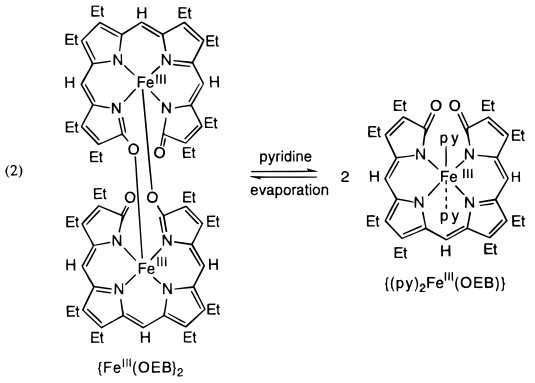

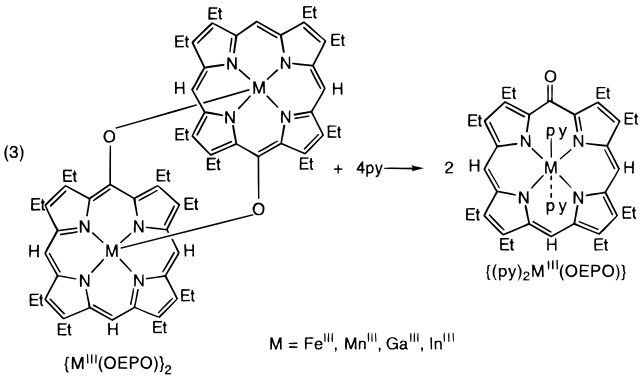

of methanol or pyridine comes from the changes seen in the ^1H NMR spectra and their temperature dependencies, which are more nearly Curie-like in the presence of methanol, the increase in the magnetic moments for the complexes in the presence of methanol, and the alteration seen in the electrochemistry when methanol is present.

The properties of $\{Fe^{II}(OEBOMe)\}_2$ in dichloromethane solution suggest that the dimeric structure remains intact in this solvent. Thus, the magnetic properties of $\{Fe^{II}(OEBOMe)\}_2$, *i.e.* the magnetic moment of 4.1 μ_B and the non-Curie behavior of the ^1H NMR spectrum, suggest that the complex contains high-spin iron(II) sites that are weakly anti-ferromagnetically

(30) Balch, A. L.; Noll, B. C.; Zovinka, E. P. *J. Am. Chem. Soc.* **1992**, *114*, 3380.
(31) Balch, A. L.; Noll, B. C.; Phillips, S. L.; Reid, S. M.; Zovinka, E. P. *Inorg. Chem.* **1993**, *32*, 4730.
(32) Balch, A. L.; Manzzanti, M.; Noll, B. C.; Olmstead, M. M. *Inorg. Chem.* **1993**, *32*, 4737.
(33) Balch, A. L.; Latos-Grażyński, L.; Noll, B. C.; Olmstead, M. M.; Zovinka, E. P. *Inorg. Chem.* **1992**, *31*, 2248.
(34) Balch, A. L.; Noll, B. C.; Reid, S. M.; Zovinka, E. P. *Inorg. Chem.* **1993**, *32*, 2610.
(35) Balch, A. L.; Noll, B. C.; Olmstead, M. M.; Reid, S. M. *J. Chem. Soc., Chem. Commun.* **1993**, 1088.
(36) Balch, A. L.; Koerner, R.; Latos-Grażyński, L.; Noll, B. C. *J. Am. Chem. Soc.* **1996**, *118*, 2760.
(37) Goff, H. M.; Shimomura, E. T.; Lee, Y. J.; Scheidt, W. R. *Inorg. Chem.* **1984**, *23*, 315.
(38) Godziela, G. M.; Tilotta, D.; Goff, H. M. *Inorg. Chem.* **1986**, *25*, 2142.
(39) Wojaczynski, J.; Latos-Grażyński, L. *Inorg. Chem.* **1995**, *34*, 1044.
(40) Wojaczynski, J.; Latos-Grażyński, L. *Inorg. Chem.* **1995**, *34*, 1054.
(41) Wojaczynski, J.; Latos-Grażyński, L. *Inorg. Chem.* **1996**, *35*, 4812.
(42) Wojaczynski, J.; Latos-Grażyński, L.; Olmstead, M. M.; Balch, A. L. *Inorg. Chem.* **1997**, *36*, 4548.

coupled if the dimer persists in dichloromethane solution.[43] Additionally, the electrochemical behavior shown in Figure 8 is consistent with a dimeric structure for $\{Fe^{II}(OEBOMe)\}_2$ in dichloromethane solution. However, there is also the possibility that a rapid dimer/monomer equilibrium exists in dichloromethane solution. Dimeric systems such as $\{M^{III}(OEB)\}_2$[4] and $[\{M^{III}(OEPO)\}_2]^n$ ($n = 0$ or $1+$)[29,44] with two paramagnetic centers generally show significant variation in the line widths of the methylene resonances with the broadest resonances assigned to the protons that are closest to the second paramagnetic center. However, the ^{1}H NMR spectrum from a dichloromethane solution of $\{Fe^{II}(OEBOMe)\}_2$ (Trace A of Figure 6) shows sixteen methylene resonances with very similar line widths. Thus, this spectrum lacks one of the characteristic features found in several other related dimers, but it must also be noted that the dimers that display variations in line widths are all iron(III) dimers whereas $\{Fe^{II}(OEBOMe)\}_2$ contains Fe(II). While a variety of dimeric structures are observed for model complexes, dimerization of this sort is not likely to be significant in the process of heme degradation where the protein environment keeps the individual hemes and their degradation products spatially separated.

The results presented here indicate that oxygen-based nucleophiles can attack verdohemes to produce ring-opened products which can be detected and characterized. The process of verdoheme hydrolysis is likely to proceed from **1** to **3** followed by rapid ring opening to yield **4** as observed here. The partial positive charge at the 5-oxa position of the verdoheme macrocycle facilitates nucleophilic attack on the adjacent carbon atoms.

It remains to be seen what factors control the position of additions of other nucleophiles to verdohemes. Simple amines can be expected to add to the verdoheme macrocycle rather than to the metal, since it is known that ammonia reacts with verdoheme to form a 5-azaporphyrin.[45] Thiols are also suspected to add to the 5-oxaporphyrin macrocycle, but it remains to be determined conclusively whether the resulting adducts have structure **3** or **4**.[20] Additions of methoxide to $[Zn^{II}(OEOP)]^+$ and $[Co^{II}(OEOP)]^+$ have recently been shown to form ring-opened monomers with structrure **4** and four-coordinate metal centers.[21,46]

The spectroscopic data presented here should facilitate the identification of the open chain tetrapyrroles with structure **4** in chemical reactions and in proteins. Verdoheme must be converted to biliverdin before the tetrapyrrole is released from heme oxygenase. The results described here make it possible to detect the ring-opened tetrapyrrole with iron still coordinated. Thus this work sets the stage for more detailed examination of the course of the transformation of verdoheme to biliverdin in heme degrading proteins where it is possible that verdoheme could be attacked by a serine residue and covalently affixed to the protein. Characteristic features of the open chain tetrapyrrole complex **4** include the remarkable low energy absorption feature that are seen in the UV/vis spectra in Figure 5 and specific ^{1}H NMR spectral features. The latter include downfield shifts for the tetrapyrrole methylene (and by inference methyl) protons and the meso protons and upfield shifts for protons adjacent to the oxygen atom.

Table 3. Crystallographic Data for $\{Fe^{II}(OEBOMe)\}_2$

formula	$C_{36}H_{46}FeN_4O_2$	γ, deg	90
formula wt ($g\cdot mol^{-1}$)	622.62	V, Å^3	3191(2)
		Z	4
color and habit	blue plate	T, K	130(2)
crystal system	monoclinic	d_{calcd}, $g\cdot cm^{-3}$	1.296
space group	$P2_1/n$	radiation, (λ Å)	Cu Kα 1.54178
a, Å	13.477(6)	μ, mm^{-1}	4.083
b, Å	13.836(6)	range of transmission factors	0.57 to 0.69
c, Å	17.128(5)		
α, deg	90	R1[a]	0.064
β, deg	92.47(3)	wR2[b]	0.158

[a] $R1 = \sum||F_o| - |F_c||/\sum|F_o|$. [b] $wR2 = [\sum[w(F_o^2 - F_c^2)^2]/\sum[w(F_o^2)^2]]^{1/2}$.

Experimental Section

Preparation of Compounds. The iron complexes of octaethyl-5-oxaporphyrin were prepared as described previously.[1]

Methoxide Additions to Iron Verdohemes. All iron verdoheme samples and methoxide solutions were prepared and sealed in dioxygen free solvents under a dinitrogen atmosphere in a glovebox. Solutions of sodium methoxide were produced by saturating a methanol solution with solid sodium methoxide. Solutions of sodium methoxide-d_3 were prepared by dissolution of 100 μL of 40 wt % KOD/D_2O in 2 mL of methanol-d_4. Reactions with either methoxide source produced similar results, but the addition of proteo methoxide introduces an overwhelming ^{1}H NMR signal from the added methoxide. NMR titrations with these methoxide solutions into a septum sealed NMR tube that contained a solution of the appropriate iron complex were performed with a 10 or 100 μL syringe. Sample concentrations for the iron complexes were on the order of 1 to 3 mM and typically required 2 to 20 μL of methoxide solution for complete conversion.

Preparation and Isolation of $\{Fe^{II}(OEBOMe)\}_2$. In a dinitrogen-filled glovebox, a 32.4 mg (5.0×10^{-2} mmol) sample of $Cl_2Fe^{III}(OEOP)$ was reduced to $ClFe^{II}(OEOP)$ with sodium dithionite as described previously.[1] The sample of $ClFe^{II}(OEOP)$ was dissolved in 10 mL of methanol to produce a rich green solution. A 1 mL portion of a methanol solution that was saturated with sodium methoxide was added to the verdoheme solution. The solution lightened in color to give a yellow green solution. The volume of the solution was reduced by one-half by evaporation under vacuum. After standing for 12 h, the microcrystalline solid was collected by filtration and washed with methanol to give 12.2 mg (40%) of black crystals of $\{Fe^{II}(OEBOMe)\}_2$. The sample may be recrystallized by dissolution in dichloromethane followed by the addition of methanol and partial evaporation of the solvent.

Preparation of Meso-Deuterated Complexes. A 342.7 mg (0.611 mmol) sample of Mg^{II}(OEP-meso-d_4) was prepared via a known route[47] and transmetalated by reaction with $Fe^{II}Cl_2\cdot 4H_2O$ to produce $ClFe^{III}$(OEP-meso-d_4). Subsequently, $ClFe^{III}$(OEP-meso-d_4) was converted into Cl_2Fe^{III}(OEOP-meso-d_3) by coupled oxidation in dichloromethane/pyridine with ascorbic acid as reductant as described earlier[1] with a yield of 131 mg (33%).

X-ray Data Collection for $\{Fe^{II}(OEBOMe)\}_2$. A deep blue plate of $\{Fe^{II}(OEBMe)\}_2$ was obtained by spontaneous crystallization of the complex from the methanol solution from which it was prepared. The datum crystal was coated with a light hydrocarbon oil and mounted in the 130 K dinitrogen stream of a Siemens P4 rotating anode diffractometer equipped with a low-temperature device. Crystal data and data collection parameters are given in Table 3. Two check reflections showed less than a 2% decay during the data collection. The data were corrected for Lorentz and polarization effects.

Solution and Refinement for $\{Fe^{II}(OEBOMe)\}_2$. Calculations were performed with SHELXTL-97. Scattering factors for neutral atoms and corrections for anomalous dispersion were taken from a

(43) Further analysis of the magnetic data to attempt to estimate coupling between the two iron sites is not warranted, since it is possible that even in dichloromethane solution there is some (unknown) degree of dissociation of the dimer.

(44) Balch, A. L.; Latos-Grażyński, L.; St. Claire, T. N. *Inorg. Chem.* **1995**, *34*, 1395.

(45) Balch, A. L.; Olmstead, M. M.; Safari, N. *Inorg. Chem.* **1993**, *32*, 291 and references therein.

(46) Latos-Grażyński, L.; Johnson, J. A.; Attar, S.; Olmstead, M. M.; Balch, A. L. *Inorg. Chem.* **1998**, in press.

(47) Bonnett, R.; Gale, I. A. D.; Stephenson, G. F. *J. Chem. Soc. C* **1967**, 1169.

standard source.[48] The initial solution was obtained via a Patterson map. Hydrogen atoms were added to the structure through the use of the HFIX routine and their thermal parameters were fixed to the atom to which they were attached (1.2 U for meso and methylene hydrogen atoms and 1.5 U for methyl hydrogen atoms). After an absorption correction was applied to the data,[49] all non-hydrogen atoms were refined anisotropically except for C(5) and C(10), which behaved poorly when refined anisotropically. The complete table of atomic positional parameters and a full table of bond lengths and angles for both data sets have been placed in the Supporting Information.

Instrumentation. ^{1}H NMR spectra were recorded on a General Electric QE-300 FT NMR operating in the quadrature mode (^{1}H frequency is 300 MHz). Typical spectra were collected over a 30 kHz spectral window with 8 K complex points, 256 to 2048 transients, and a repetition rate of 2.5 transients/s. The signal-to-noise ratio was improved by apodization of the free induction decay. The residual ^{1}H resonances of the deuterated solvents were used as secondary references.

The ^{2}H NMR spectra were recorded on a General Electric QE-300 operating at 46 MHz. Typical spectra were recorded over a 4 kHz spectral window with 2 K complex points, 512 to 2048 transients, and a repetition rate of 1.6 transients/s. The signal-to-noise ratio was improved by apodization of the free induction decay. Spectra were referenced to the residual ^{2}H NMR resonance of the solvent used.

Electrochemical measurements were recorded on a BioAnalytical Systems CV-50W potentiostat. All measurements were conducted at room temperature under a dinitrogen atmosphere with 0.1 M tetrabutylammonium perchlorate as the supporting electrolyte, a gold disk (0.75 mm radius) working electrode, Ag/Ag^+ reference electrode, and a platinum foil auxiliary electrode. Cyclic voltammograms were collected with a 100 or 200 mV/s sweep rate. Osteryoung square wave voltammograms were collected with a 25 mV sweep width amplitude, 15 Hz sweep width frequency, 4 mV step potential, and a 2 s quiet time.

Electronic spectra were obtained on a Hewlett-Packard 8452A diode-array spectrometer and a Hitashi U-2000 spectrometer.

Magnetic susceptibilities were determined by the Evans technique.[50]

Acknowledgment. We thank the NIH (GM-26226) for financial support, Dr. Nasser Safari for key assistance in the initial stages of this project, Dr. K. Winkler for assistance with the voltammetry, Dr. Marilyn M. Olmstead for assistance with the crystallography, and James Johnson for helpful discussions.

Supporting Information Available: Tables of X-ray structural information on $\{Fe^{II}(OEBOMe)\}_2$ (11 pages print/PDF). An X-ray crystallographic file, in CIF format, is available through the Web only. See any current masthead page for ordering information and Web access instructions.

JA980558V

(48) *International Tables for X-ray Crystallography*; Kynoch Press: Birmingham, England, 1974; Vol. 4.

(49) Parkin, S.; Moezzi, B.; Hope, H. *J. Appl. Crystallogr.* **1995**, *28*, 53.

(50) Evans, D. F.; James, T. A. *J. Chem. Soc., Dalton Trans.* **1979**, 723.